Exciton-Wave Packet Dynamics in Molecular Aggregates Studied with Pump−Probe Spectroscopy†

Mats Dahlbom,‡,§ Tatsuya Minami,‡ Vladimir Chernyak,‡ Tõnu Pullerits,§ Villy Sundström,*,§ and Shaul Mukamel*,‡

Department of Chemistry, University of Rochester, Rochester, New York 14627, and Department of Chemical Physics, Lund University, Box 124, 211 00 Lund, Sweden

Received: November 23, 1999

The doorway−window representation of sequential pump−probe spectroscopy, derived by solving the nonlinear exciton equations, is used to study exciton dynamics in molecular aggregates. Exciton relaxation is incorporated through a multilevel Redfield relaxation superoperator calculated using the Brownian oscillator spectral density for the collective phonon coordinates. Optical pulses are included using a mixed time and frequency domain (Wigner spectrogram) representation. Numerical results are presented for a five-chromophore model aggregate.

I. Introduction

The Frenkel exciton model is widely used in the description of elementary optical excitations of molecular aggregates and macromolecules[1,2] where interactions between the basic units, the chromophores, are purely Coulombic. The exciton is a quasiparticle consisting of an electron and a hole constrained to reside on the same chromophore, undergoing a wavelike motion that ideally covers the whole aggregate. The real-space Green function representation of the optical response functions offers a simple and intuitive physical picture of the energetics and dynamics of exciton systems.[3] A small set of exciton variables can be defined that completely encapsulates the exciton dynamics and naturally truncates the hierarchy generated by the Heisenberg equation of motion for a given nonlinear spectroscopic method. It has been demonstrated that the time-domain signal to third-order in the driving field can be partitioned into a short-time (coherent) and a long-time (sequential) component.[3] The former decays on the dephasing time scale τ_D whereas the latter decays on the time scale of the exciton population (fluorescence) lifetime τ_f, which is typically orders of magnitude longer. A third important time scale is the relaxation time τ_r for the exciton population to reach the Boltzmann distribution in the excited state. Typically we have $\tau_D, \tau_r \ll \tau_f$. The coherent and sequential contributions are clearly distinct when $\tau_r \gg \tau_D$. When $\tau_r \sim \tau_D$, exciton dephasing and population relaxation are simultaneous and these two componenets are not clearly separated.

The possible time-domain two-dimensional (2D) four-wave mixing techniques in molecular aggregates have been surveyed in ref 4. For certain techniques such as the two-pulse photon echo, the exciton density matrix does not have a population period and, therefore, the sequential component does not contribute and the signal is represented solely by its coherent component. Pump−probe spectroscopy depends on both components. When the time delay τ between the excitation pulses satisfies $\tau \sim \tau_D$, the signal is dominated by its coherent component. This case has been considered in our earlier work.[4] For $\tau \gg \tau_D$, the signal is sequential. If $\tau_r \ll \tau \ll \tau_f$, the exciton populations relax to a thermal equilibrium, and the signal saturates as a function of τ and only depends on the probe frequency. This case has been considered in ref 5.

In this article we build upon and expand these earlier results to calculate the pump−probe spectra for a molecular aggregate consisting of N three-level chromophores. We focus on the sequential contribution to the response function obtained with well-separated pulses. The earlier work,[5] which assumed a fully thermalized one-exciton density matrix, is extended to include exciton relaxation processes. Our approach makes use of the Green function representation of the third-order optical response derived by solving the nonlinear exciton equations (NEE),[3] where exciton transport is incorporated using the Redfield relaxation superoperator. The NEE offer significant conceptual and numerical advantages for computing the nonlinear optical response, compared with the more conventional sum-over-states (SOS) approach. They limit the computational effort to the one-exciton manifold, whose size scales as the number of molecules, N, while the SOS requires the full set of N^2 one- and two-exciton states. The NEE further avoids calculating dark states that do not contribute to the optical response and results in compact expressions that do not suffer from the almost cancellation of large terms in the SOS approach.[2] All nonlinear spectroscopic techniques can be formulated using the Green function representation of the exciton variables computed perturbatively order by order in the external field.

The most widely used description of time-resolved pump−probe spectroscopy treats the measurement as a sequence of two separate linear experiments. First the pump−pulse perturbs the system, preparing it in a nonstationary state that is subsequently monitored by the probe. By varying the pump/probe time delay, we can follow the evolution of the initially created state. This simple picture has been put to a solid mathematical foundation by the doorway−window representation of sequential pump−probe experiments performed with well-separated pulses.[2] This picture was first developed by Yan and Mukamel for describing the nuclear density matrix for vibrations and a solvent bath[6] and was extended to molecular aggregates and exciton wave packets in refs 4, 7, and 8. The doorway−window representation offers an intuitive physical

† Part of the special issue "Harvey Scher Festschrift".
‡ University of Rochester.
§ Lund University.

10.1021/jp994172y CCC: $19.00
Published on Web 03/09/2000

picture of the process and lends itself to a clear interpretation; the system interacts twice with the pump, creating the initial doorway wave packet (a particle in the excited state and a hole in the ground state). This exciton wave packet then propagates during the time delay between the pulses, whereby the exciton−bath interaction affects the exciton density matrix. The system then interacts twice with the probe, and the signal can be computed as the Liouville space overlap of the propagated doorway with the window wave packet.[5]

Pump−probe spectroscopy is conceptually very similar to the time- and frequency-resolved fluorescence technique. The pump−probe signal S_{pp} contains the fluorescence signal as one of the components, known as the stimulated emission contribution. The DW representation for the time- and frequency-gated fluorescence using the same level of theory as implemented in this paper has been developed in ref 9. In this paper we extend these results to pump−probe spectroscopy.

The DW picture of pump−probe spectroscopy divides the generation of the signal into three steps: (i) the formation of the exciton DM representing the exciton populations and coherences (this process is described by the doorway wave packet, (ii) propagation of the exciton DM during the pump/probe delay period, and (iii) formation of the signal as a result of scattering of an exciton created by the probe field with excitons created by the pump. This process is described by projecting the window function onto the exciton density matrix obtained at the end of step ii. The propagation operator for the reduced density matrix (step ii) contains the exciton−bath interaction modeled by the multilevel Redfield theory.[10−15] This theory assumes a vibrational bath coupled linearly to the exciton system. The Redfield superoperator contains population relaxation (T_1), coherence relaxation (T_2), and mixed terms. The operator was computed using the Brownian oscillator model for the collective bath coordinates[16] under the rotating wave approximation. It conserves the number of excitons and satisfies detailed balance, leading to a thermally equilibrated exciton distribution at long times. The window wave packet depends on the one-exciton Green function, as well as the exciton−exciton scattering matrix, derived from the two-exciton variable[2] using the Bethe−Salpeter equation.[17] This matrix completely avoids the computationally expensive calculation of the two-exciton manifold. It carries all information about the two-exciton manifold, its energy levels, and anharmonicities relevant for optical nonlinearities. It is straightforward to verify from the structure of this matrix that the scattering contributions and the entire nonlinear response vanish for a system of three-level chromophores that have a harmonic ladder structure.

The excitation pulses are incorporated through their Wigner spectrograms,[18−21] a mixed time and frequency representation, which interpolate naturally between the pure time and frequency domain descriptions and can account for arbitrary pulse shapes and durations. In an ideal pump−probe measurement, the pulses are short compared to the exciton dynamics time scale and long compared to the inverse line width. In this case, known as the snapshot limit, the signal, S_{pp}^0, does not depend on the pulse envelopes. More generally, the spectra are obtained by convoluting the snapshot signal with the pump and the probe spectrograms, making it possible to dress the wave packets with pulses of arbitrary shapes and durations once the snapshot spectrum has been calculated.[2]

The paper is organized as follows: the formal expressions for the pump−probe signal are summarized in section II, and numerical applications to a model linear pentamer (J-aggregate)

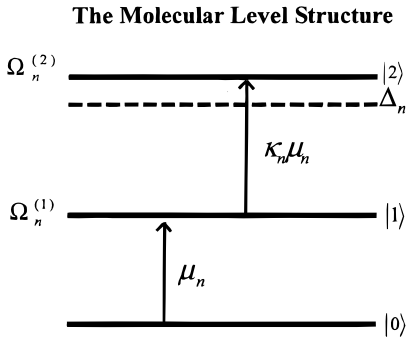

Figure 1. Three-level molecular structure for the nth chromophore and parameters. The first excited-state $|1\rangle$ has the energy $\Omega_n^{(1)}$ and the second excited-state $|2\rangle$ with $\Omega_n^{(2)} = 2\Omega_n^{(1)} + \Delta_n$. The anharmonicity parameter, Δ_n, represents the deviation from a harmonic ladder. The transition dipole for the $|0\rangle \rightarrow |1\rangle$ transition is denoted μ_n and for the $|1\rangle \rightarrow |2\rangle$ transition $\mu_n' = \kappa_n\mu_n$.

in the snapshot limit are presented and discussed in section III. For clarity, all the derivations are given in the appendices. The pump−probe signal is derived in Appendix D using the optical response function of Appendix A. The exciton−exciton scattering matrix is defined in Appendix B, and the Redfield superoperator is derived in Appendix C. The Wigner spectrograms are given in Appendix E, and the snapshot limit spectrum is presented in Appendix F.

II. Doorway−Window Representation of Pump−Probe Spectroscopy

We consider a molecular aggregate made out of N interacting three-level chromophores (Figure 1). $\Omega_n^{(1)}$ is the first excited state for the nth molecule, and $\Omega_n^{(2)}$ is the doubly excited electronic state. $\kappa_n \equiv \mu_n'/\mu_n$ is the ratio of the transition dipole strengths of the $|1\rangle \rightarrow |2\rangle$ (μ_n') and $|0\rangle \rightarrow |1\rangle$($\mu_n$) transitions of the chromophore.[22] The anharmonicity parameter, $\Delta_n \equiv \Omega_n^{(2)} - 2\Omega_n^{(1)}$, represents the level structure deviation from a harmonic ladder.

This aggregate can be represented by the Frenkel exiton Hamiltonian:

$$H \equiv H_e + H_{ph} + H_{int} - E(t)\hat{P} \tag{2.1}$$

H_e describes the electronic system

$$H_e = \sum_{mn} h_{mn}\hat{B}_m^\dagger \hat{B}_n + \sum_n \frac{g_n}{2}(\hat{B}_n^\dagger)^2(\hat{B}_n)^2 \tag{2.2}$$

where $h_{mn} = \Omega_m^{(1)}\delta_{mn} + J_{mn}$, and J_{mn} is the intermolecular dipole−dipole interaction in the Heitler−London approximation. The parameter

$$g_n \equiv 2\hbar(\kappa_n^{-2}\Omega_n^{(2)} - \Omega_n^{(1)})$$

contains all information about the two-exciton manifold. The exciton creation (annihilation) operators $\hat{B}_m^\dagger$ ($\hat{B}_m$) add (remove) an excitation on the mth chromophore and satisfy the Pauli commutator relations

$$[\hat{B}_n, \hat{B}_m^\dagger] = \delta_{mn}[1 - (2 - \kappa_n^2)\hat{B}_n^\dagger \hat{B}_n] \tag{2.3}$$

In the case of two-level chromophores $\kappa_n = 0$, and eq 2.2 prohibits two excitons from occupying the same chromophore site at any given time.

The exciton states are defined by the eigenvalues (ϵ_α) and eigenvectors (φ_α) of the Hamiltonian

$$\sum_n h_{mn}\varphi_\alpha(n) = \epsilon_\alpha\varphi_\alpha(m) \tag{2.4}$$

$\varphi_\alpha(m)$ represent the transformation between the real-space (chromophore) representation to the delocalized exciton-space representation.

The harmonic phonon bath Hamiltonian is

$$H_{\mathrm{ph}} = \sum_\nu \left(\frac{p_\nu^2}{2m_\nu} + \frac{m_\nu\omega_\nu^2 q_\nu^2}{2}\right) \tag{2.5}$$

and the system−bath interaction is taken to be

$$H_{\mathrm{int}} = \sum_{\nu,n} q_\nu \bar{\Omega}_{n,\nu} \bar{B}_n^\dagger \bar{B}_n \tag{2.6}$$

where q_ν, p_ν, m_ν, and ω_ν are the coordinate, momentum, mass, and frequency, of the νth bath oscillator, respectively.

Using projection operator techniques, we can trace out the bath coordinates from the full density matrix.[3,15] H_{ph} and H_{int} then generate the relaxation superoperator (see Appendix C) for the reduced excitonic density matrix. The last term in eq 2.1 describes the coupling between the system and the external electromagnetic field, where the polarization operator is given by

$$\hat{P} = \sum_n \mu_n(\hat{B}_n^\dagger + \hat{B}_n) \tag{2.7}$$

The sequential pump−probe signal is derived in Appendices A−E and is given by

$$S_{\mathrm{pp}}(\tau, \bar{\omega}_2) = \sum_{mnkl}\int_0^\infty \mathrm{d}\tau' \int_0^\infty \mathrm{d}t_2\, W_{mn}(\tau - \tau', \bar{\omega}_2)\, G^{(N)}_{mn,kl}(t_2)\, D_{kl}(\tau' - t_2, \bar{\omega}_1) \tag{2.8}$$

Here $\bar{\omega}_1$ ($\bar{\omega}_2$) are the pump (probe) carrier frequencies and τ is the pump/probe delay period. D_{kl} is the doorway wave packet, representing the exciton density matrix prepared by the pump. W_{mn} is the window wave packet created from the ground, the one-, and the two-exciton states, by two interactions with the probe. $G^{(N)}$ represents the propagation of the doorway wave packet during the delay period between pump and probe.

This representation provides an intuitive physical description that separates the process into a preparation, propagation, and detection of the excitonic wave packet. The doorway wave packet is the reduced one-exciton density matrix containing the initially prepared exciton populations and coherences. The signal is given by the Liouville space overlap of this wave packet, propagated for the delay period, with the window. The bleach signal comes from the hole−hole overlap in the ground state, and stimulated emission and excited-state absorption come from particle−particle overlap in the excited state.

The derivation of eq 2.8 starts with the basic expression for the nonlinear response function presented in Appendix A. It is given in terms of the one-exciton Green function, $G(\omega)$, the exciton−exciton scattering matrix, $\bar{\Gamma}(\omega)$, and the density matrix propagator, $G^{(N)}(t)$. $\bar{\Gamma}$ is given in Appendix B. Closed expressions for $G^{(N)}$ are derived in Appendix C using the Redfield superoperator in Liouville space. The doorway−window form eq 2.8 is then derived in Appendix D, and the pump and the probe pulses are expressed in terms of their Wigner spectrograms in Appendix E.

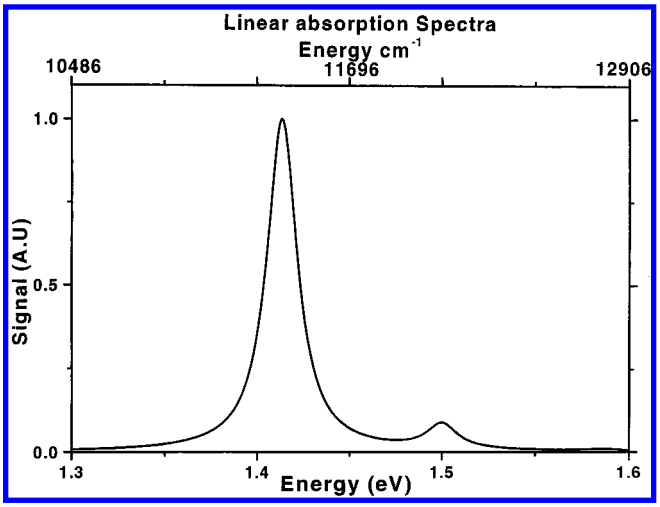

Figure 2. Linear absorption spectra for the model pentamer. The five chromophores are identical with single excited molecular energy 1.5 eV and $\Delta_n = 0.1$ eV. The transition dipoles are set in a head-to-tail arrangement with dipole moments 1.0. The dipole coupling between neighboring chromophores were all set to $J = -0.05$ eV, and all other couplings were set to zero. The exciton dephasing rate, Γ, in eqs A6−A7, is set to 81 cm^{-1}.

The calculations are simplified considerably in the snapshot limit where the laser pulses are short compared with the exciton dynamics time scale and long compared with the electronic dephasing time scale.[2,6,17] In this limit we can assume the pulses to be both monochromatic and very short in the time domain, and the doorway and the window become simpler, since the time integrations in eq 2.8 can be carried out. The pump−probe signal then assumes the form

$$S^0_{\mathrm{pp}}(\bar{\omega}_2, \tau; \bar{\omega}_1) = \sum_{mnkl} W^{\,0}_{mn}(\bar{\omega}_2)\, G^{(N)}_{mn,kl}(\tau)\, D^0_{kl}(\bar{\omega}_1) \tag{2.9}$$

where all snapshot quantities, labeled by a 0 superscript, are defined in Appendix F. The numerical calculation presented below are made in the snapshot limit.

III. Numerical Results and Discussion

We have computed the pump−probe spectrum of a linear model aggregate made of five identical chromophores with first excited state energy $\Omega_n^{(1)} = 1.5$ eV and all transition dipoles in a head-to-tail arrangement along the aggregate axis. We assumed $\Delta_n = 0.1$ eV, $\mu_n = 1$, and $\kappa_n = 0.7$ for all five molecules[22] (see Figure 1).

The overdamped Brownian oscillator model for the bath was used for computing the Redfield matrix, with the following approximations: We assume that the various chromophores are coupled to identical and uncorrelated baths and that each chromophore is only coupled to a single collective bath coordinate. The resulting Redfield relaxation superoperator is given in Appendix C. This model contains two parameters: the nuclear relaxation time scale, Λ^{-1}, and the exciton−phonon coupling strength, λ. Their ratio, Λ/λ, has to be greater than 1 in order for the Redfield theory to apply. Room temperature, $T = 300$ K, is assumed in all calculations.

This model has a one-exciton manifold with three allowed states separated by two forbidden states. The one-exciton energies (in eV) are 1.413, 1.450, 1.500, 1.550, and 1.587. The linear absorption spectrum is shown in Figure 2. The lowest

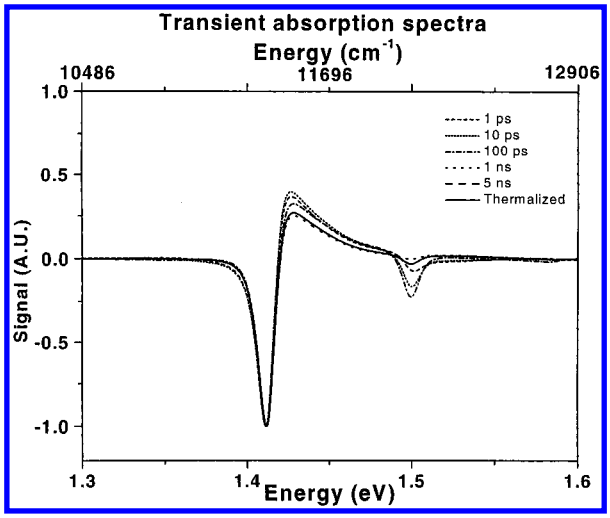

Figure 3. Transient absorption (pump−probe) spectra for the aggregate using six time delays, as indicated. The inverse nuclear relaxation time $\Lambda = 50$ cm^{-1}, and the exciton−phonon coupling $\lambda = 0.1$ cm^{-1}. Other parameters are given in the Figure 2 caption and in the text. Excitation is resonant with the highest one-exciton state. The temperature $T = 300$ K.

one-exciton state carries most of the transition dipole strength. The lowest, third, and fifth exciton states carry approximately 92.4%, 7.0%, and 0.5%, respectively, of the oscillator strength. The second and fourth states are dark.

The transient pump−probe absorption spectra consist of photobleaching (PB), stimulated emission (SE), and excited-state absorption (ESA). The PB and SE arise from the depletion of the ground state and populating the one-exciton states, whereas the ESA comes from the transition from the one-exciton to the two-exciton manifold. These two contributions are close in frequency owing to the nearly harmonic chromophore level structure. In the SOS calculations these contributions are calculated separately. In the present formulation, they are lumped together and computational cost is greatly reduced since we avoid the explicit calculation of the two-exciton eigenstates and their transition dipole elements.

The pump−probe spectra for six time delays when the pump is tuned to the highest one-exciton state are shown in Figure 3. We see PB from the two lowest allowed one-exciton states; the third is too weak to be clearly visible on this scale. The positive ESA contribution to the signal originates from the different one-exciton states. Initially we excite the highest one-exciton level, and the exciton wave packet is nonthermal. The higher exciton levels have a large population, as is clearly visible in the ESA. As the time delay increases, the ESA decays owing to population relaxation toward thermal equilibrium, and the coherences dephase. The ground-state PB does not change with time, since molecules have been excited from the common ground state to the one-exciton manifold. The apparent difference in PB signal in the vicinity of the second lowest level (∼1.5 eV) reflects the decay of ESA owing to the thermalization of the exciton-state population. Finally, the long-time spectra represent the thermalized DM.

We have further calculated the propagated doorway wave packet in the exciton basis

$$N_{\alpha\beta}(\tau) \equiv \sum_{\gamma\delta} G^{(N)}_{\alpha\beta,\gamma\delta}(t_2)\, D^0_{\gamma\delta}(\tau - t_2, \bar{\omega}_1) \qquad (3.1)$$

In Figure 4 we display the absolute values of $N_{\alpha\beta}(\tau)$ as a function of time delay, corresponding to the pump−probe

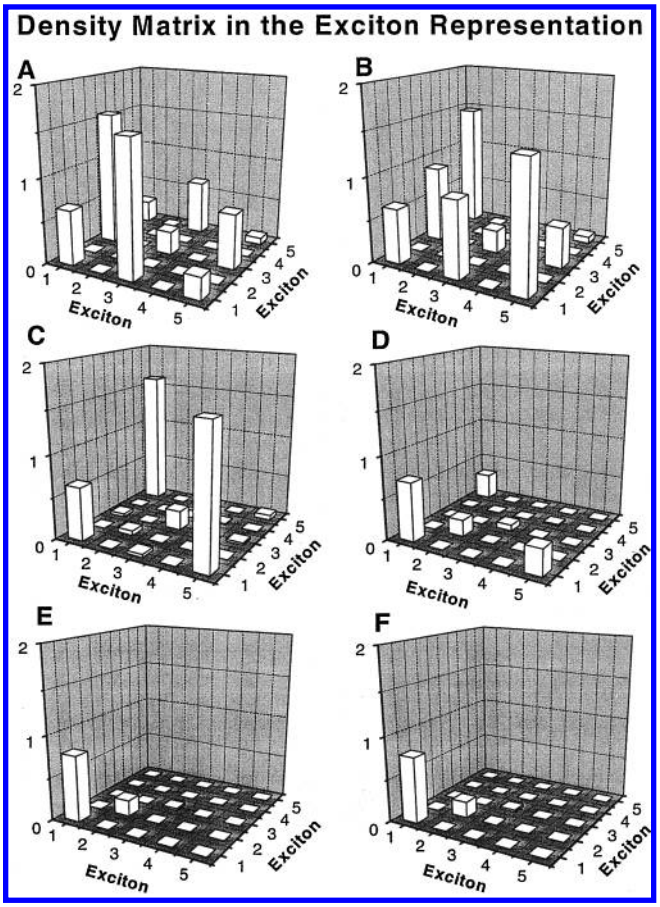

Figure 4. Propagated doorway wave packets displayed in the exciton-space representation for the spectra shown in Figure 3. Panels A−F correspond to the six time delays of Figure 3.

spectra shown in Figure 3. The exciton wave packet contains populations of all allowed states and strong coherences (i.e., off-diagonal DM elements) between these states. Panel A in the top left corner displays the exciton wave packet at short time delay (1 ps). At longer times (panels B−E), we see how the coherences dephase and vanish, while the populations relax toward the lowest one-exciton state. The coherences dephase on a faster time scale compared to population relaxation, and exciton−phonon coupling further populates the optically forbidden states. The last two panels show that at long times the propagated density matrix (panel E) reaches thermal equilibrium (panel F). Initially the pump pulse creates a nonequilibrium doorway wave packet that is propagated using the Redfield relaxation operator leading eventually to a diagonal density matrix with Boltzmann distributed populations. The time evolution of the absolute magnitude of the various matrix elements of the doorway wave packet of Figure 4 normalized to a unit trace is displayed in Figure 5. The off-diagonal and diagonal elements are shown in panels A and B, respectively. We note that N_{13} and N_{35} dephase much faster than N_{15}.

In summary, the sequential pump−probe signal of the molecular aggregate was expressed in the doorway−window representation. Linear absorption, pump−probe transient absorption spectra, and the time-dependent density matrix were presented and analyzed for a model system.

Acknowledgment. The support of the National Science Foundation is gratefully acknowledged. M.D would thanks the Royal Physiografic Society in Lund, Sweden, and the Sweden−America Foundation for his fellowship.

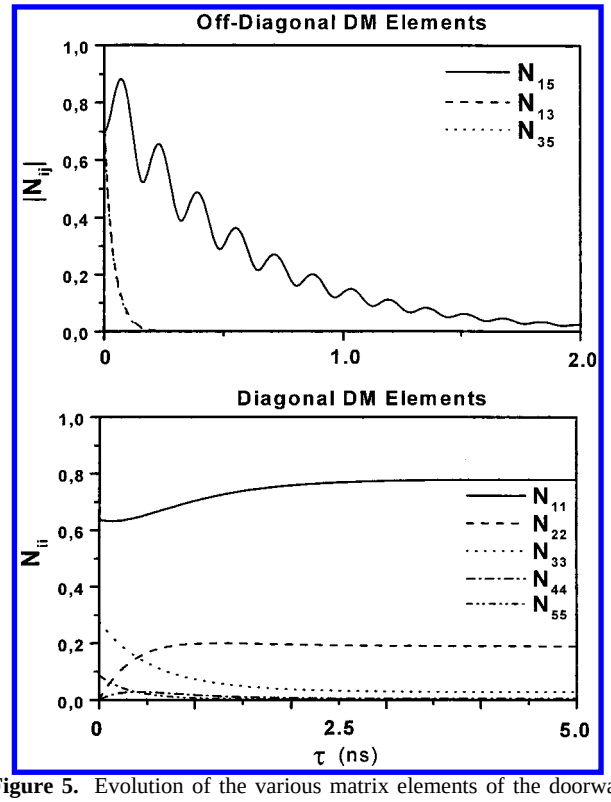

Figure 5. Evolution of the various matrix elements of the doorway wave packet shown in Figure 4.

Appendix A. Green Function Expression for the Pump−Probe Signal

In the pump−probe technique the electric field is given by

$$E(t) = E_1(t)\exp(-i\bar{\omega}_1 t) + E_2(t-\tau)\exp(-i\bar{\omega}_2 t) + \text{c.c.} \tag{A1}$$

with the pump−pulse envelope $E_1(t)$ centered around $t = 0$, and the probe−pulse envelope $E_2(t - \tau)$ centered around $t = \tau$. The corresponding carrier frequencies are $\bar{\omega}_1$ and $\bar{\omega}_2$, respectively.

The pump−probe signal S_{pp} can be written in terms of the probe field $E_2(t)$ and the third-order polarization $P^{(3)}(t)$ (ref 2)

$$S_{pp}(\tau, \bar{\omega}_2) = \text{Re}\int_{-\infty}^{\infty} dt\, E_2^*(t-\tau)\, P^{(3)}(t)\exp(i\bar{\omega}_2 t) \tag{A2}$$

Using the response function (eqs 4.17 and 4.18 of ref 3), $P^{(3)}(t)$ can be written for well-separated pulses

$$P^{(3)}(t) = \int_0^{\infty} dt_3 \int_0^{\infty} dt_2 \int_0^{\infty} dt_1\, R^i(t_3, t_2, t_1)\, E(t-t_3)\, E(t-t_3-t_2)\, E(t-t_3-t_2-t_1) \tag{A3}$$

where $R^i(t_3, t_2, t_1) = R_1^i(t_3, t_2, t_1) + R_2^i(t_3, t_2, t_1)$, with (ref 3)

$$R_1^i(t_3, t_2, t_1) = 2\sum \mu_q\mu_p\mu_k\mu_r \int_0^{t_3} d\tau'' \int_0^{\tau''} d\tau'\, G_{qs}(\tau')\, T_{js,i'r',jj'}(\tau''-\tau')\, G_{r'r}(t_3-\tau'')\, \bar{G}_{i'j',kl}(t_3+t_2-\tau'')\, G_{lp}^*(t_1) + c.c. \tag{A4}$$

$$R_2^i(t_3, t_2, t_1) = 2\sum \mu_q\mu_l\mu_p\mu_r \int_0^{t_3} d\tau'' \int_0^{\tau''} d\tau'\, G_{qs}(\tau')\, T_{js,i'r',jj'}(\tau''-\tau')\, G_{r'r}(t_3-\tau'')\, \bar{G}_{i'j',kl}(t_3+t_2-\tau'')\, G_{kp}(t_1) + \text{c.c.} \tag{A5}$$

The two contributions (Eqs A4 and A5) correspond to the left and right Feynman diagrams given in Figure 6, respectively.

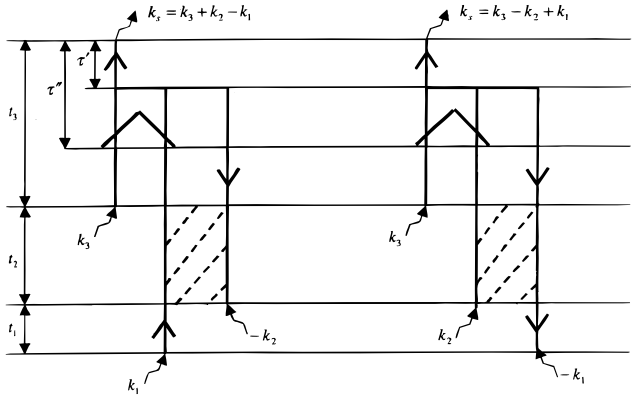

Figure 6. Feynman diagrams representing the sequential pump−probe spectrum with well-separated pulses: left diagram eq A4; right diagram, eq A5. See ref 3 for notation.

The one-exciton Green function representing the propagator of the exciton variables $\langle\hat{B}\rangle$ is defined as

$$G_{mn}(t) = i\theta(t)\,\langle m|e^{-iH_e t-\Gamma t}|n\rangle \tag{A6}$$

or equivalently in the frequency domain (after a Fourier transform)

$$G_{mn}(\omega) = -\sum_{\alpha}\frac{\varphi_\alpha(m)\,\varphi_\alpha(n)}{\omega-\epsilon_\alpha+i\Gamma} \tag{A7}$$

where Γ is the exciton dephasing rate.

The auxiliary T function related to the exciton−exciton scattering matrix is calculated in Appendix B.

Appendix B. The Exciton−Exciton Scattering Matrix

In this Appendix we present expressions for the exciton scattering matrix $\bar{\Gamma}$ and the auxiliary function T.

For the present model (eqs 2.1−2.3) the exciton scattering matrix $\bar{\Gamma}_{jj',pp'}$ has the form[23]

$$\bar{\Gamma}_{jj',pp'}(\omega_2+\tilde{\epsilon}_\gamma) = \delta_{jj'}\delta_{pp'}\bar{\Gamma}_{jp}^{(0)}(\omega_2+\tilde{\epsilon}_\gamma) \tag{B1}$$

with

$$\bar{\Gamma}_{jp}^{(0)}(\omega_2+\tilde{\epsilon}_\gamma) = [F(\omega_2+\tilde{\epsilon}_\gamma)]_{jp}^{-1}[(\hbar(\omega_2+\tilde{\epsilon}_\gamma)+g_p)\kappa^2 - 2\hbar(\omega_2+\tilde{\epsilon}_\gamma)] \tag{B2}$$

where

$$F_{jp}(\omega_2+\tilde{\epsilon}_\gamma) = \delta_{jp}\kappa^2 - [(\hbar(\omega_2+\tilde{\epsilon}_\gamma)+g_j-2i\Gamma)\kappa^2 - 2\hbar(\omega_2+\tilde{\epsilon}_\gamma)]G_{jp}^{(2)}(\omega_2+\tilde{\epsilon}_\gamma) \tag{B3}$$

and the unperturbed two-exciton Green function

$$G_{jp}^{(2)}(\omega_2+\tilde{\epsilon}_\gamma) = \frac{1}{\hbar}\sum_{\alpha\beta}\frac{\varphi_\alpha(j)\,\varphi_\beta(j)\,\varphi_\alpha(p)\,\varphi_\beta(p)}{\omega_2+\epsilon_\gamma-\epsilon_\alpha-\epsilon_\beta+3i\Gamma} \tag{B4}$$

The T function in eq A4 is defined as

$$T_{js,i'r',jj'}(\tau''-\tau') \equiv \tilde{\Gamma}_{js,i'r'}(\tau''-\tau')\, G_{jj'}^*(\tau''-\tau') \tag{B5}$$

where $\bar{\Gamma}(\tau''-\tau')$ is the exciton−exciton scattering matrix and $G^*(\tau''-\tau')$ the complex conjugated one-exciton Green function. Owing to the localized form of the commutation relations for the exciton creation (annihilation) operators, eq 2.3, the scat-

tering matrix, $\bar{\Gamma}$, can be expressed as an $N \times N$ matrix instead of as a tetradic $N^2 \times N^2$

$$T_{js,i'r',jj'}(\tau'' - \tau') = \delta_{js}\delta_{i'r'}T_{ji'j'}(\tau'' - \tau') \quad \text{(B6)}$$

where we have introduced the following compact notation

$$T_{ji'j'}(\tau'' - \tau') = \bar{\Gamma}^{(0)}_{ji'}(\tau'' - \tau')\, G^*_{jj'}(\tau'' - \tau') \quad \text{(B7)}$$

The scattering matrix enters the window wave packet through the auxiliary function, $T(\omega)$, defined as the product of the scattering matrix, $\bar{\Gamma}$, and the one-exciton Green, G

$$T_{jpj'}(\tau'' - \tau') \equiv \bar{\Gamma}_{jp}(\tau'' - \tau')\, G^*_{jj'}(\tau'' - \tau') \quad \text{(B8)}$$

This can be written in frequency domain as a convolution[5]

$$T_{jpj'}(\omega_2) = \int_{-\infty}^{\infty} \frac{d\epsilon}{2\pi i}\, \bar{\Gamma}_{jp}(\omega_2 + \epsilon)\, G^*_{jj'}(\epsilon) \quad \text{(B9)}$$

All the poles of the scattering matrix are in the lower half of the complex plane, while the complex conjugated one-exciton Green function has its poles in the upper half. Using the theorem of residues and closing the contour in the upper half-plane, we obtain

$$T_{jpj'}(\omega_2) = \sum_{\gamma} \varphi_\gamma(j)\, \varphi_\gamma(j')\, \bar{\Gamma}_{jp}(\omega_2 + \tilde{\epsilon}_\gamma) \quad \text{(B10)}$$

where $\tilde{\epsilon}_\gamma = \epsilon_\gamma + i\Gamma$) are the poles of the Green function.

Equation B10 is the final expression for the auxiliary function, used in computing the window wave packet, eqs D13 and D14.

Appendix C. The Redfield Relaxation Superoperator

The Green function $G^{(N)}$ is obtained by solving the Redfield equation. This Green function propagates the doorway wave packet from the initial preparation, through the time delay t_2, to the instant when the system interacts with the probe pulse.

The exciton−phonon interaction is taken into account, to second order using a projection operator technique and tracing over the bath coordinates.[3] This results in a set of equations for the coupled variables whose formal solution yields the relaxation superoperators for the corresponding exciton variables (for a detailed derivation see ref 3). The reduced equation of motion for the density matrix, in the one-exciton basis

$$\frac{dN_{\alpha'\beta'}(t)}{dt} = -i\omega_{\alpha'\beta'}N_{\alpha'\beta'}(t) - \sum_{\alpha\beta} \bar{R}_{\alpha'\beta',\alpha\beta}N_{\alpha\beta}(t) \quad \text{(C1)}$$

where $\omega_{\alpha'\beta'} = (\epsilon_{\alpha'} - \epsilon_{\beta'})$, has the formal solution[11] $N(t) \equiv G^{(N)}(t)\, N(0)$.

We next transform the Green function for the exciton variables, N, from the exciton to the molecular basis

$$G_{mn,kl}{}^{(N)}(t) \equiv \sum_{\alpha\beta,\gamma\delta} \varphi_\alpha(m)\, \varphi_\beta(n)\, \varphi_\gamma(k)\, \varphi_\delta(l)\, G^{(N)}_{\alpha\beta,\gamma\delta}(t) \quad \text{(C2)}$$

In our earlier work,[3,6] we have represented the Green function $G^{(N)}$ in terms of its irreducible part $\bar{G}_{mn,kl}(t)$

$$G^{(N)}_{mn,kl}(t) \equiv G_{mk}(t)\, G^\dagger_{nl}(t) + \bar{G}_{mn,kl}(t) \quad \text{(C3)}$$

However, in the sequential contribution considered here the pulse separation is larger than the dephasing time, the first term in the right-hand side of eq C3 vanishes, and we can replace $\bar{G}$ by $G^{(N)}$.

Introducing the set of collective bath coordinates

$$\bar{q}_{mn} = \sum_\nu m_\nu \omega_\nu^2 (\delta_{mn}\bar{\Omega}_{n,\nu} + J_{mn,\nu})q_\nu \quad \text{(C4)}$$

the spectral density is defined as the Fourier transform of the correlation function of collective coordinates[16]

$$C_{mn,kl}(\omega) = \int_{-\infty}^{\infty} dt\, \exp(i\omega t)\, \langle [\bar{q}_{mn}(t), \bar{q}_{kl}(0)] \rangle \quad \text{(C5)}$$

We adopt the following simple model for the relaxation. Each chromophore has its own heat bath with one collective bath coordinate, and the various collective coordinates are completely uncorrelated. We further assume that these baths have identical spectral densities, implying a single exciton−phonon coupling constant λ, instead of a set of $\lambda_{\alpha,ij}$. We then have for the spectral density $C_{mn,kl}(\omega) = \delta_{mn}\delta_{kl}\delta_{mk}C_m(\omega)$, where $C_m(\omega) = C_{mn,mn}(\omega)$. The phonon Green function[3] can be written in the exciton basis

$$M_{\alpha\beta,\gamma\delta}(t) = \frac{1}{2}\int_{-\infty}^{\infty} \frac{d\omega}{2\pi}\, C_{\alpha\beta,\gamma\delta}(\omega)\, [\coth(\omega/2kT)\cos(\omega t) - i\sin(\omega t)] \quad \text{(C6)}$$

where

$$C_{\alpha\beta,\gamma\delta}(\omega) \equiv \sum_{mn,kl} \varphi_\alpha(m)\, \varphi_\beta(n)\, \varphi_\gamma(k)\, \varphi_\delta(l)\, C_{mn,kl}(\omega) \quad \text{(C7)}$$

We next assume the spectral density of a single strongly overdamped Brownian oscillator[2,4]

$$C_m(\omega) = 2\lambda \frac{\Lambda\omega}{\Lambda^2 + \omega^2} \quad \text{(C8)}$$

where Λ^{-1} is the nuclear relaxation time.

The phonon Green function can then be expressed as[2]

$$M_{\alpha\beta,\gamma\delta}(t) = \Psi_{\alpha\beta\gamma\delta}M(t) \quad \text{(C9)}$$

and

$$\Psi_{\alpha\beta\gamma\delta} \equiv \sum_m \varphi_\alpha(m)\, \varphi_\beta(m)\, \varphi_\gamma(m)\, \varphi_\delta(m) \quad \text{(C10)}$$

$$M(t) = \lambda\Lambda\left[\cot\left(\frac{\Lambda}{2kT}\right)\exp(-\Lambda t) + 4kT\sum_{n=1}^{\infty} \frac{\nu_n \exp(-\nu_n t)}{\nu_n^2 - \Lambda^2} - i\exp(-\Lambda t)\right] \quad \text{(C11)}$$

where $\nu_n \equiv 2\pi nkT$ are the Matsubara frequencies.

For this model, the Redfield tensor is given by

$$\bar{R}_{\alpha'\beta',\alpha\beta} = \int_0^\infty R_{\alpha'\beta',\alpha\beta}(t)\exp(i\omega_{\alpha\beta}t)\, dt \quad \text{(C12)}$$

where $\omega_{\alpha\beta} \equiv \epsilon_\alpha - \epsilon_\beta$, and

$$R_{\alpha'\beta',\alpha\beta}(t) = -\sum_\gamma \exp(i\omega_{\beta\gamma}t)\, M_{\alpha\gamma,\gamma\alpha'}(t)\delta_{\beta\beta'} + \exp(i\omega_{\beta\alpha'}t)\, M_{\alpha\alpha',\beta\beta'}(t) - \sum_\gamma \exp(i\omega_{\gamma\alpha}t)\, M^*_{\beta\gamma,\gamma\beta'}(t)\delta_{\alpha\alpha'} + \exp(i\omega_{\beta'\alpha}t)\, M^*_{\beta\beta',\alpha\alpha'}(t) \quad \text{(C13)}$$

The Redfield tensor is finally given by $\bar{R}_{\alpha'\beta',\alpha\beta} = R^{+}_{\alpha'\beta',\alpha\beta} + \bar{R}^{+}_{\alpha'\beta',\alpha\beta} + R^{-}_{\alpha'\beta',\alpha\beta} + \bar{R}^{-}_{\alpha'\beta',\alpha\beta}$ where

$$R^{+}_{\alpha'\beta',\alpha\beta} = -\lambda\Lambda \sum_{\gamma} \Psi_{\gamma\alpha\gamma\alpha'}\left[\left(\cot\left(\frac{\Lambda}{2kT}\right) - i\right) \mathrm{Y}_{\alpha\gamma}(\Lambda) + 4kT \sum_{n=1}^{\infty} \frac{\nu_n}{\nu_n^2 - \Lambda^2} \mathrm{Y}_{\alpha\gamma}(\nu_n)\right]\delta_{\beta\beta'}$$

$$\bar{R}^{+}_{\alpha'\beta',\alpha\beta} = \lambda\Lambda\Psi_{\alpha\beta\alpha'\beta'}\left[\left(\cot\left(\frac{\Lambda}{2kT}\right) - i\right) \mathrm{Y}_{\alpha\alpha'}(\Lambda) + 4kT \sum_{n=1}^{\infty} \frac{\nu_n}{\nu_n^2 - \Lambda^2} \mathrm{Y}_{\alpha\alpha'}(\nu_n)\right]$$

$$\bar{R}^{-}_{\alpha'\beta',\alpha\beta} = \lambda\Lambda\Psi_{\alpha\beta\alpha'\beta'}\left[\left(\cot\left(\frac{\Lambda}{2kT}\right) + i\right) \mathrm{Y}_{\beta'\beta}(\Lambda) + 4kT \sum_{n=1}^{\infty} \frac{\nu_n}{\nu_n^2 - \Lambda^2} \mathrm{Y}_{\beta'\beta}(\nu_n)\right]$$

$$R^{-}_{\alpha'\beta',\alpha\beta} = -\lambda\Lambda \sum_{\gamma} \Psi_{\gamma\beta\gamma\beta'}\left[\left(\cot\left(\frac{\Lambda}{2kT}\right) + i\right) \mathrm{Y}_{\gamma\beta}(\Lambda) + 4kT \sum_{n=1}^{\infty} \frac{\nu_n}{\nu_n^2 - \Lambda^2} \mathrm{Y}_{\gamma\beta}(\nu_n)\right]\delta_{\alpha\alpha'} \quad \text{(C14)}$$

Here we have introduced the auxiliary function

$$\mathrm{Y}_{\alpha\beta}(Q) \equiv \frac{1}{\mathrm{Q} - i\omega_{\alpha\beta}} \quad \text{(C15)}$$

It is straightforward to verify that the population part satisfies the necessary physical requirements:[2] the conservation of probability

$$\bar{R}_{\alpha\alpha,\alpha\alpha} = -\sum_{\beta}^{\beta\neq\alpha} \bar{R}_{\beta\beta,\alpha\alpha} \quad \text{(C16)}$$

and the detailed balance, $\bar{R}_{\alpha\alpha,\beta\beta}/R_{\beta\beta,\alpha\alpha} = \exp[(-\epsilon_\alpha - \epsilon_\beta)/kT]$. The Green function for the exciton density matrix, $G^{(N)}(t_2)$ in eq 2.8, was calculated by solving eq C1 using eq C14 together with eq C3.

Appendix D. The Doorway−Window Representation

In this Appendix we derive the DW representation for the pump−probe signal. Equation (A2) may be recast in the doorway window representation, similar to the time- and frequency-gated fluorescence.[9] To that end we first shift the time origin from the generation of the signal field at the end of the third time interval to the first interaction with the probe field, at the end of the second time interval[3] (see Feynman diagrams in Figure 5). This amounts to changing τ' to $(t_3 - \tau'')$ and τ'' to $(t_3 - \tau')$, and we obtain:

$$R^{i}_{1}(t_3, t_2, t_1) = 2\sum_{qlpk} \mu_q\mu_l\mu_p\mu_k \int_0^{t_3} \mathrm{d}\tau'' \int_0^{\tau''} \mathrm{d}\tau'\, G_{qs}(t_3 - \tau'') T_{\mathrm{js},i'r',jj'}(\tau'' - \tau') G_{r'r}(\tau') \bar{G}_{i'j',kl}(t_2 + \tau') G^{*}_{lp}(t_1) \quad \text{(D1)}$$

$$R^{i}_{2}(t_3, t_2, t_1) = 2\sum_{qlpk} \mu_q\mu_l\mu_p\mu_r \int_0^{t_3} \mathrm{d}\tau'' \int_0^{\tau''} \mathrm{d}\tau'\, G_{qs}(t_3 - \tau'') T_{js,i'r',jj'}(\tau'' - \tau') G_{r'r}(\tau') \bar{G}_{i'j',kl}(t_2 + \tau') G_{kp}(t_1) \quad \text{(D2)}$$

Using the exact relation

$$G^{(N)}_{i'j',kl}(t_2 + \tau') = \sum_{mn} G^{(N)}_{i'j',mn}(\tau') G^{(N)}_{mn,kl}(t_2) \quad \text{(D3)}$$

we can separate the signal into a doorway (D), a propagation part, and a window (W)

$$S_{pp}(\tau, \bar{\omega}_2) = \sum_{mnkl} \int_{-\infty}^{\infty} \mathrm{d}t_4 \int_0^{\infty} \mathrm{d}t_2\, W_{mn}(t_4 - \tau, \bar{\omega}_2) G^{(N)}_{mn,kl}(t_2)\, D_{kl}(t_4 - t_2, \bar{\omega}_1) \quad \text{(D4)}$$

The doorway wave packet reads

$$D_{kl}(t_4 - t_2, \bar{\omega}_1) = D_{kl,L}(t_4 - t_2, \bar{\omega}_1) + D_{kl,R}(t_4 - t_2, \bar{\omega}_1) \quad \text{(D5)}$$

where the left $D_{kl,\mathrm{L}}$ and right $D_{kl,\mathrm{R}}$ components satisfy the relation

$$D_{\mathrm{L}}(t_4 - t_2, \bar{\omega}_1) = [D_{\mathrm{R}}(t_4 - t_2, \bar{\omega}_1)]^{\dagger} \quad \text{(D6)}$$

which guarantees the hermiticity of the doorway wave packet.

The window wave packet is given by

$$W_{mn}(t_4 - \tau, \bar{\omega}_2) = W_{mn,\mathrm{L}}(t_4 - \tau, \bar{\omega}_2) + W_{mn,\mathrm{R}}(t_4 - \tau, \bar{\omega}_2) \quad \text{(D7)}$$

with

$$W_{\mathrm{L}}(t_4 - \tau, \bar{\omega}_2) = [W_{\mathrm{R}}(t_4 - \tau, \bar{\omega}_2)]^{\dagger} \quad \text{(D8)}$$

The left and the right components of the doorway and window functions can be expressed in terms of their snapshot limit counterparts $D^{0}_{mn,\alpha}$ and $W^{0}_{mn,\alpha}$ and the spectrograms F_α and I_α, with $\alpha = \mathrm{L}, \mathrm{R}$. These expressions have a similar form

$$D_{\alpha}(t_4 - t_2, \bar{\omega}_1) = \int_0^{\infty} \mathrm{d}t_1 \int_{-\infty}^{\infty} \frac{\mathrm{d}\omega_1}{2\pi} D^{0}_{\alpha}(t_1) I_{\alpha}(t_4 - t_2, \bar{\omega}_1 - \omega_1) \exp(is_\alpha\omega_1 t_1) \quad \text{(D9)}$$

$$W_{\alpha}(t_4 - \tau, \bar{\omega}_2) = \int_0^{\infty} \mathrm{d}t_3 \int_{-\infty}^{\infty} \frac{\mathrm{d}\omega_3}{2\pi} W^{0}_{\alpha}(t_3) F_{\alpha}(t_4 - \tau, \omega_3 - \bar{\omega}_2) \exp(is_\alpha\omega_3 t_3) \quad \text{(D10)}$$

with $\alpha = \mathrm{L}, \mathrm{R}$ and $s_{\mathrm{L}} = -s_{\mathrm{R}} = 1$.

The doorway and the window are written in terms of G, $G^{(N)}$, and T

$$D^{0}_{kl,\mathrm{L}}(t_1) = \sum_{p} \mu_l\mu_p G_{kp}(t_1) \quad \text{(D11)}$$

$$D^{0}_{kl,\mathrm{R}}(t_1) = \sum_{p} \mu_p\mu_k G^{*}_{lp}(t_1) \quad \text{(D12)}$$

and

$$W^{0}_{mn,\mathrm{L}}(t_3) = \sum_{qr} \mu_q\mu_r \int_0^{t_3} \mathrm{d}\tau'' \int_0^{\tau''} \mathrm{d}\tau'\, G_{qs}(t_3 - \tau'') T_{js,i'r',jj'}(\tau'' - \tau') G_{r'r}(\tau') G^{(N)}_{i'j',mn}(\tau') \quad \text{(D13)}$$

$$W^{0}_{mn,\mathrm{R}}(t_3) = \sum_{qs} \mu_q \mu_r \int_0^{t_3} \mathrm{d}\tau'' \int_0^{\tau''} \mathrm{d}\tau'\, G^{*}_{qs}(t_3 - \tau'') \, T^{*}_{js,i'r',jj'}(\tau'' - \tau')\, G^{*}_{r'r}(\tau')\, G^{(N)*}_{i'j',nm}(\tau') \quad \text{(D14)}$$

We can further neglect $G^{(N)}(t)$ in the window since exciton relaxation is typically slow compared with the dephasing time scale, $G^{(N)}_{i'j',mn}(t) = \delta_{i'm}\delta_{j'n}$. Equations D13 and D14 can be recast as

$$W^{0}_{mn,L}(t_3) = \sum_{qrj} \mu_q \mu_r \int_0^{t_3} \mathrm{d}\tau'' \int_0^{\tau''} \mathrm{d}\tau' G_{qj}(t_3 - \tau'') \, T_{jmn}(\tau'' - \tau')\, G_{mr}(\tau') \quad \text{(D15)}$$

$$W^{0}_{mn,R}(t_3) = \sum_{qrj} \mu_q \mu_r \int_0^{t_3} \mathrm{d}\tau'' \int_0^{\tau''} \mathrm{d}\tau' G^{*}_{qj}(t_3 - \tau'') \, T^{*}_{jnm}(\tau'' - \tau')\, G^{*}_{nr}(\tau') \quad \text{(D16)}$$

Appendix E. Wigner Spectrograms for the Laser Fields

In this Appendix we introduce the Wigner spectrograms for the pump and the probe fields.[9] We start with the correlation function of the pump field amplitudes

$$I(\tau' - \tau'') \equiv \langle E_1(\tau')\, E_1^{*}(\tau'') \rangle \quad \text{(E1)}$$

Using this correlation function, we can represent the pump in terms of the following right, left, and Wigner spectrograms:

$$I_{\mathrm{R}}(\tau, \omega) = \int_{-\infty}^{\infty} \mathrm{d}t \exp(i\omega t)\, I(\tau, \tau + t) \quad \text{(E2)}$$

$$I_{\mathrm{L}}(\tau', \omega) = \int_{-\infty}^{\infty} \mathrm{d}t \exp(i\omega t)\, I(\tau' - t, \tau') \quad \text{(E3)}$$

$$I_{\mathrm{W}}(\tau_+, \omega) = \int_{-\infty}^{\infty} \mathrm{d}t \exp(i\omega t)\, I(\tau_+ - t/2, \tau_+ + t/2) \quad \text{(E4)}$$

Similarly, we introduce a correlation function of the probe field

$$F(\tau', \tau'') \equiv \langle E_2(\tau')\, E_2^{*}(\tau'') \rangle \quad \text{(E5)}$$

and the corresponding spectrograms

$$F_{\mathrm{R}}(\tau; \omega) = \int_{-\infty}^{\infty} \mathrm{d}t \exp(i\omega t)\, F(\tau, \tau + t) \quad \text{(E6)}$$

$$F_{\mathrm{L}}(\tau'; \omega) = \int_{-\infty}^{\infty} \mathrm{d}t \exp(i\omega t)\, F(\tau' - t, \tau') \quad \text{(E7)}$$

$$F_{\mathrm{W}}(\tau_+; \omega) = \int_{-\infty}^{\infty} \mathrm{d}t \exp(i\omega t)\, F(\tau_+ - t/2, \tau_+ + t/2) \quad \text{(E8)}$$

These definitions are used in eqs D9 and D10.

Appendix F. The Snapshot Limit for the Pump−Probe Signal

In this Appendix we present the expressions for the doorway and window functions in the snapshot limit,[18] obtained by setting

$$I_\alpha(\tau' - t_2, \omega_1 - \bar{\omega}_1) = \delta(\tau' - t_2)\, \delta(\omega_1 - \bar{\omega}_1) \quad \text{(F1)}$$

$$F_\alpha(\tau - \tau', \omega_3 - \bar{\omega}_2) = \delta(\tau - \tau')\, \delta(\omega_3 - \bar{\omega}_2) \quad \text{(F2)}$$

Equation 2.8 then assumes the form of eq 2.9, where $D^{0}_{kl}(\bar{\omega}_1)$ and $W^{0}_{mn}(\bar{\omega}_2)$ are the Fourier transforms of $D^{0}_{kl}(t_1)$ and $W^{0}_{mn}(t)$

$$D^{0}_{kl}(\bar{\omega}_1) \equiv \int_{-\infty}^{\infty} \mathrm{d}t_1\, \mathrm{e}^{i\bar{\omega}_1 t_1} D^{0}_{kl}(t_1) \quad \text{(F3)}$$

$$W^{0}_{mn}(\bar{\omega}_2) \equiv \int_{-\infty}^{\infty} \mathrm{d}t\, \mathrm{e}^{i\bar{\omega}_2 t} W^{0}_{mn}(t) \quad \text{(F4)}$$

here

$$D^{0}_{kl}(t_1) = D^{0}_{kl,\mathrm{L}}(t_1) + D^{0}_{kl,\mathrm{R}}(t_1) \quad \text{(F5)}$$

and

$$W^{0}_{mn}(t_3) = W^{0}_{mn,\mathrm{L}}(t_3) + W^{0}_{mn,\mathrm{R}}(t_3) \quad \text{(F6)}$$

$D^{0}_{kl,\alpha}(t)$ and $W^{0}_{mn,\alpha}(t)$ for $\alpha = \mathrm{L}, \mathrm{R}$ are given by eqs D11 − D14.

References and Notes

(1) Davydov, A. S. *Theory of Molecular Excitons*; McGraw-Hill Book Company: New York, 1962.

(2) Mukamel, S. *Principles of Nonlinear Optical Spectroscopy*; Oxford University Press: New York, 1995.

(3) Chernyak, V.; Zhang, W. M.; Mukamel, S. *J. Chem. Phys.* **1998**, *109*, 9587.

(4) Zhao, Y.; Chernyak, V.; Mukamel, S. *J. Phys. Chem. A* **1998**, *102*, 6614.

(5) Meier, T.; Chernyak, V.; Mukamel, S. *J. Phys. Chem. B* **1997**, *101*, 7332.

(6) Yan, Y. J.; Mukamel, S. *Phys. Rev. A* **1990**, *41*, 6485.

(7) Zhang, W. M.; Meier, T.; Chernyak, V.; Mukamel, S. *J. Chem. Phys.* **1998**, *108*, 7763.

(8) Renger, T.; May, V. *J. Phys. Chem. B* **1997**, *101*, 7232. Renger, T.; May, V. *Phys. Rev. Lett.* **1997**, *78*, 3408. Renger, T.; Voigt, J.; May, V.; Kühn, O. *J. Phys. Chem.* **1996**, *100*, 15654.

(9) Chernyak, V.; Minami, T.; Mukamel, S. *J. Chem. Phys.*, in press.

(10) Redfield, A. G. *IBM J. Res.* **1957**, *1*, 19.

(11) Pollard, W. T.; Felts, A. K.; Friesner, R. A. *Adv. Chem. Phys.* **1997**, *93*, 77. Pollard, W. T.; Friesner, R. A. *J. Chem. Phys.* **1994**, *100*, 5054.

(12) Jean, J. M.; Friesner, R. A.; Fleming, G. R. *J. Chem. Phys.* **1992**, *96*, 5827.

(13) de Bree, P.; Wiersma, D. A. *J. Chem. Phys.* **1979**, *70*, 790.

(14) Blum, K. *Density Matrix Theory and Applications*; Plenum Press: New York, 1981.

(15) Chernyak, V.; Mukamel, S. *J. Opt. Soc. Am. B* **1996**, *13*, 1302.

(16) Chernyak, V.; Mukamel, S. *J. Chem. Phys.* **1996**, *105*, 4565.

(17) Chernyak, V.; Mukamel, S. In *Notions and Perspectives of Nonlinear Optics*; Keller, O., Ed.; *World Scientific*: Singapore, 1996; Vol. 93.

(18) Mukamel, S. *J. Chem. Phys.* **1997**, *107*, 4165.

(19) Mukamel, S.; Ciordas-Ciurdariu, C.; Khidekel, V. *IEEE J. Quantum Electron.* **1996**, *32*, 1278.

(20) Trebino, R.; DeLong, K. D.; Fittinghoff, D. N.; Sweetser, J. N.; Krumbügel M. A.; Richman, B. A. *Rev. Sci. Instrum.* **1997**, *68*, 9.

(21) Dugan, M.; Tull, J. X.; Warren, W. S. *Ultrafast Phenomena X*; Barbara, P. F., Fujimoto, J. G., Knox, W. H., Zinth, W., Eds.; Springer Verlag: New York, 1996.

(22) As outlined in ref 3, there is a freedom in the choice of the parameter κ_n in eq 2.3, which reflects a freedom of choice of the basic quantum variables (i.e., the operators $\hat{B}_n$, $\hat{B}_n^{\dagger}$). It has been shown in ref 3 that the most convenient choice of κ_n corresponds to the situation when the molecular dipole operator is linear in the $\hat{B}_n$, $\hat{B}_n^{\dagger}$ operators. In this case κ_n is given by the ratio of the $|1\rangle \rightarrow |2\rangle$ and $|0\rangle - |1\rangle$ transition dipoles.

(23) Kühn, O.; Chernyak, V.; Mukamel, S. *J. Chem. Phys.* **1996**, *105*, 8586.